UC Davis
UC Davis Previously Published Works

Title

Multi-hypothesis comparison of Farquhar and Collatz photosynthesis models reveals the unexpected influence of empirical assumptions at leaf and global scales

Permalink

Journal

ISSN

Authors

Walker, Anthony P
Johnson, Abbey L
Rogers, Alistair
et al.

Publication Date

DOI

Copyright Information

Peer reviewed

PRIMARY RESEARCH ARTICLE

Global Change Biology WILEY

Multi-hypothesis comparison of Farquhar and Collatz photosynthesis models reveals the unexpected influence of empirical assumptions at leaf and global scales

Anthony P. Walker[1] | Abbey L. Johnson[1] | Alistair Rogers[2] |
Jeremiah Anderson[2] | Robert A. Bridges[3] | Rosie A. Fisher[4,5] | Dan Lu[6] |
Daniel M. Ricciuto[1] | Shawn P. Serbin[2] | Ming Ye[7]

[1]Environmental Sciences Division and Climate Change Science Institute, Oak Ridge National Laboratory, Oak Ridge, TN, USA

[2]Environmental & Climates Sciences Department, Brookhaven National Laboratory, Upton, NY, USA

[3]Cyber & Applied Data Analytics Division, Oak Ridge National Laboratory, Oak Ridge, TN, USA

[4]National Center for Atmospheric Research, Boulder, CO, USA

[5]Centre Européen de Recherche et de Formation Avancée en Calcul Scientifique (CERFACS), Toulouse, France

[6]Computational Sciences & Engineering Division, Oak Ridge National Laboratory, Oak Ridge, TN, USA

[7]Department of Earth, Ocean, and Atmospheric Science, Florida State University, Tallahassee, FL, USA

Correspondence
Anthony P. Walker, Environmental Sciences Division and Climate Change Science Institute, Oak Ridge National Laboratory, 1 Bethel Valley Rd., Oak Ridge, TN 37831-6301, USA.
Email: walkerap@ornl.gov

Abstract

Mechanistic photosynthesis models are at the heart of terrestrial biosphere models (TBMs) simulating the daily, monthly, annual and decadal rhythms of carbon assimilation (A). These models are founded on robust mathematical hypotheses that describe how A responds to changes in light and atmospheric CO_2 concentration. Two predominant photosynthesis models are in common usage: Farquhar (FvCB) and Collatz (CBGB). However, a detailed quantitative comparison of these two models has never been undertaken. In this study, we unify the FvCB and CBGB models to a common parameter set and use novel multi-hypothesis methods (that account for both hypothesis and parameter variability) for process-level sensitivity analysis. These models represent three key biological processes: carboxylation, electron transport, triose phosphate use (TPU) and an additional model process: limiting-rate selection. Each of the four processes comprises 1–3 alternative hypotheses giving 12 possible individual models with a total of 14 parameters. To broaden inference, TBM simulations were run and novel, high-resolution photosynthesis measurements were made. We show that parameters associated with carboxylation are the most influential *parameters* but also reveal the surprising and marked dominance of the limiting-rate selection *process* (accounting for 57% of the variation in A vs. 22% for carboxylation). The limiting-rate selection assumption proposed by CBGB smooths the transition between limiting rates and always reduces A below the minimum of all potentially limiting rates, by up to 25%, effectively imposing a fourth limitation on A. Evaluation of the CBGB smoothing function in three TBMs demonstrated a reduction in global A by 4%–10%, equivalent to 50%–160% of current annual fossil fuel emissions. This analysis reveals a surprising and previously unquantified influence of a process that has been integral to many TBMs for decades, highlighting the value of multi-hypothesis methods.

See also Commentary on this article by Chris and Rebecca, 27, 716–718.

1 | INTRODUCTION

As the gateway for carbon entry into terrestrial ecosystems, photosynthesis plays the keystone role in the biosphere of transferring atmospheric CO_2 into terrestrial ecosystems. Since its inception 40 years ago the Farquhar et al. (1980; hereafter FvCB) model of C3 photosynthesis has revolutionized photosynthesis research (>5,000 citations, at time of writing). The FvCB model describes photosynthetic carbon assimilation (A) using a set of mathematically described hypotheses that represent the enzymatic subprocesses of photosynthesis and their integration, including: light-stimulated electron transport, CO_2 fixation in the Calvin–Benson cycle and photorespiration. The FvCB model is an integrated set of mathematically described hypotheses, a system hypothesis, that yields quantitative predictions to accurately describe the dynamics of A in response to incident radiation (I), carbon dioxide concentration (C_a) and temperature. Observation, experiment and model-based photosynthesis research has seen substantive advances due to the availability of this mathematically rigorous hypothesis. However, variants of the FvCB model exist, chief among them is that proposed by Collatz

et al. (1991; hereafter CBGB). Differing hypotheses for three key subprocesses distinguish the models: (a) electron transport, (b) limiting process selection, and (c) triose phosphate use (TPU).

Terrestrial biosphere models (TBMs)—which simulate global land ecosystems and their role in the Earth System—rely on the FvCB and CBGB models (as well as various hybrids and additions to these core models) to simulate leaf-scale photosynthesis and its response to global change, in particular, increasing C_a. The CBGB model and hybrids with the FvCB model are employed by several prominent TBMs (Table 1; e.g. IBIS, JULES, CLM and ELM; Clark et al., 2011; Foley et al., 1996; Oleson et al., 2013). Yet despite the keystone role of photosynthesis in the biosphere and the wide variation in TBM simulations of photosynthesis (Anav et al., 2015; Rogers, Medlyn, et al., 2017), a rigorous, quantitative comparison of the FvCB and CBGB models has not been undertaken. In part this is because rigorous methods to compare and evaluate competing sets of hypotheses have not been available until recently.

Sensitivity analysis (SA) is used to determine the sensitivity of model output to variability in individual model components. Variability in model output can be introduced through a number of

TABLE 1 Factorial list of possible models from the given hypotheses

Model	Carboxylation	TPU	Limiting-rate selection	Electron transport	TBMs, etc.
M1111	1. Equations (1), (4) and (5)	1. Absent	1. Equation (2)	1. Equation (6a)	FvCB,[a] ORCHIDEE
M1211	1	2. Equation (7)	1	1	
M1121	1	1	2. Equations (3a,b)	1	
M1221	1	2	2	1	CLM4.5,[b] FATES,[b] ELM[b]
M1112	1	1	1	2. Equation (6b)	SDGVM; BETHY
M1212	1	2	1	2	
M1122	1	1	2	2	
M1222	1	2	2	2	
M1113	1	1	1	3. Equation (6c)	
M1213	1	2	1	3	CLM4.0,[b] LM3[b]
M1123	1	1	2	3	
M1223	1	2	2	3	CBGB,[b] CTEM,[b] IBIS,[c] JULES[b]

Abbreviations: TBMs, terrestrial biosphere models; TPU, triose phosphate use.

[a]Strictly speaking FvCB used a different electron transport model but it was quickly superseded by Equation (6a) in 1984 and the original is not widely used.

[b]While all of these models assume TPU limitation, they all assume $\alpha_{tpu} = 0$ so that TPU limited $A = 3TPU$.

[c]IBIS uses a unique TPU formulation (Foley et al., 1996).

sources (Beven, 2016), two key sources are parameter choice and differences in mathematical representations of the multiple processes that a model simulates, e.g. photosynthetic electron transport. SA methods to assess model sensitivity to various *parameters* in TMBs are common (e.g. Dietze et al., 2014; Gupta & Razavi, 2018; Koven et al., 2019; Ricciuto et al., 2018; Zaehle et al., 2005) while SA methods to assess model output sensitivity to alternative *process representations* are rare. Parameter SA methods can be applied in the context of multiple models and sensitivity indexes averaged to get an overall assessment of parameter influence under model uncertainty (Dai & Ye, 2015). However, these methods miss a key element of model output variability—the difference in the means among models, or between-model variation. Parameter SA can only account for within-model variation, necessitating a process SA that is designed to account for both within (parameter) *and* between (process representation) model variation (e.g. Dai et al., 2017).

A further obstacle to rigorous process SA is that the majority of commonly used modelling codes are not sufficiently flexible to switch between all of the various hypotheses for all of the various processes under investigation. The Multi-Assumption Architecture and Testbed (MAAT) has been designed to overcome this issue (Walker et al., 2018). MAAT is a hyper-modular, multi-hypothesis modelling framework designed to easily pose multiple alternative models by combining alternative mathematically described hypotheses for the processes that form the building blocks of a model, or system hypothesis (Walker et al., 2018). Through hyper-modularity MAAT allows a factorial combination of each hypothesis across all processes and subprocesses, exploring the full range of possible models and ensuring that each representation of each process is evaluated against all other representations for all other processes, i.e. it is fully comprehensive. MAAT's ability to combine models at the scale of individual process hypotheses enables the application of rigorous process (SA) algorithms, such as that of Dai et al. (2017) which was designed to work with modelling codes like MAAT.

In this study we use MAAT to formally compare the leaf-scale enzyme-kinetic models of C3 photosynthesis by comparing the FvCB and CBGB model formulations. The choice of electron transport model, limiting-rate selection, TPU limitation and parametric variability are examined. We ask the questions: (a) which processes are most influential for simulating carbon assimilation at various levels of atmospheric CO_2 concentration and incident radiation, (b) which parameters are most influential, and (c) are the influential process and parameters different when considering absolute assimilation or the response of assimilation to a change in CO_2? We further evaluate the outcome of this SA using global TBM simulations and measurements of leaf-scale photosynthesis.

1.1 | Comparison of the FvCB and CBGB models of photosynthesis

Enzyme-kinetic models of photosynthesis (Farquhar et al., 1980) simulate net CO_2 assimilation (A—μmol CO_2 m^{-2} s^{-1}) in response to

CO_2 concentrations in the intercellular airspace of the leaf (C_i—Pa) and incident photosynthetically active radiation (I—μmol photons m^{-2} s^{-1}). The model scales the gross carbon assimilation rate (A_g—μmol CO_2 m^{-2} s^{-1}) to account for photorespiration, minus 'dark' respiration (R_d—μmol CO_2 m^{-2} s^{-1}):

$$A = A_g \left(1 - \Gamma_* / C_i\right) - R_d, \tag{1}$$

where Γ_* is the photorespiratory CO_2 compensation point (Pa), the C_i at which A_g is equal to the rate of CO_2 release from oxygenation. A_g is simulated as a change point model (Gu et al., 2010) where one of two (FvCB) or three (CBGB) potentially limiting processes ($A_{c,g}$, $A_{j,g}$, and $A_{p,g}$—μmol CO_2 m^{-2} s^{-1}), described in detail below, are selected. FvCB simply identifies the minimum of the potentially limiting rates:

$$A_g = min \left\{A_{c,g}, A_{j,g}, A_{p,g}\right\}, \tag{2}$$

resulting in discontinuities in the derivative of the A–C_i or A–I curves at the change points where $A_{c,g} = A_{j,g}$ and $A_{j,g} = A_{p,g}$. In order to '*introduce a more realistic, gradual transition from one limitation to another, and to allow for some co-limitation*', CBGB proposed non-rectangular hyperbolic (quadratic) smoothing between the three potentially limiting rates:

$$0 = \theta_{cj} A_{cj,g}^2 - \left(A_{c,g} + A_{j,g}\right) A_{cj,g} + A_{c,g} A_{j,g}, \tag{3a}$$

$$0 = \theta_{cjp} A_g^2 - \left(A_{cj,g} + A_{p,g}\right) A_g + A_{cj,g} A_{p,g}, \tag{3b}$$

where $A_{cj,g}$ is a latent variable resulting from smoothing between $A_{c,g}$ and $A_{j,g}$. Parameters θ_{cj} and θ_{cjp} (θ and β in CBGB's original notation) are curvature parameters that take a value 0–1 with lower values leading to greater smoothing. The FvCB method is a special case of the CBGB method where both θ_{cj} and θ_{cjp} take the value 1, while if θ_{cj} and θ_{cjp} take the value 0 smoothing becomes rectangular hyperbolic (Johnson & Thornley, 1984).

$A_{c,g}$, $A_{j,g}$ and $A_{j,g}$ are modelled as Michaelis–Menten functions of C_i. For $A_{c,g}$, V_{cmax} (μmol CO_2 m^{-2} s^{-1}) determines the asymptote:

$$A_{c,g} = \frac{V_{cmax} C_i}{C_i + K_c \left(1 + O_i / K_o\right)}, \tag{4}$$

where O_i is the internal O_2 partial pressure (kPa), and K_c (Pa) and K_o (kPa) are the Michaelis–Menten half-saturation constants of the RuBisCO enzyme for CO_2 and for O_2. For $A_{j,g}$, the asymptote is proportional to the electron transport rate (J—μmol e m^{-2} s^{-1}) where:

$$A_{j,g} = \frac{J}{4} \frac{C_i}{\left(C_i + 2\Gamma_*\right)}, \tag{5}$$

A number of hypotheses to represent J exist, most commonly used are the following three. Based on Smith (1937), two representations of J saturate at a maximum electron transport rate (J_{max}), (a) Farquhar and Wong (1984) used non-rectangular smoothing (Equation 6a), (b) Harley et al. (1992) use an alternative non-rectangular hyperbola

(Equation 6b), while (c) CBGB proposed a linear model that has no maximum (Equation 6c) respectively:

$$0 = \theta_j J^2 + a\alpha_i I J_{max} J + a\alpha_i I J_{max}, \tag{6a}$$

$$J = \frac{a\alpha_i I}{\left[1 + \left(\frac{a\alpha_i I}{J_{max}}\right)^2\right]^{0.5}}, \tag{6b}$$

$$J = a\alpha_i I, \tag{6c}$$

where a is the leaf absorptance (the fraction of I absorbed by the leaf, unitless), α_i is the intrinsic quantum efficiency of electron transport (the number of electrons transported per absorbed photon, e photon^{-1}) and θ_j is a non-rectangular hyperbola smoothing parameter. $a\alpha_i$ is the apparent quantum efficiency of electron transport (electrons transported per incident photon). Following FvCB, in this study we define α_i as $0.5(1 - f)$, where f is the fraction of photons absorbed by the leaf but not absorbed by the light harvesting complexes, and 0.5 represents the requirement of two photons for full linear transport of a single electron.

Subsequent to the development of the FvCB model, a third potential limitation was identified under high C_a and high irradiance (I). TPU in sucrose and starch synthesis releases phosphate needed for the regeneration of RuBP, thus low rates of sucrose and starch synthesis can limit RuBP regeneration and therefore A (Sharkey, 1985). CBGB proposed this additional rate-limiting cycle in their model ($A_{p,g}$), which was refined (von Caemmerer, 2000) to account for reversed sensitivities of A to C_i and O_i in the TPU limiting state (Harley & Sharkey, 1991):

$$A_{p,g} = \frac{3TPU\, C_i}{C_i + (1 + 3\alpha_{tpu})\, \Gamma_*}, \tag{7}$$

where α_T is the fraction of glycolate exported but not returned to the chloroplast during photorespiration. CBGB assumed a closed photorespiratory cycle ($\alpha_T = 0$) such that multiplication by the first term in Equation (1) yields 3TPU.

2 | METHODS

As described above, the MAAT (Walker et al., 2018; https://github.com/walkeranthonyp/MAAT) is a hyper-modular, multi-hypothesis modelling framework. MAAT is written in R (R Core Team, 2020) and provides a general framework and code structure for building models that allows for new processes to be added easily. Higher-level 'system models' integrate multiple processes into a coherent representation of a given system. A number of these system models have been coded into MAAT and in this study we use the leaf-scale enzyme-kinetic model of photosynthesis (Walker et al., 2018). MAAT also encodes process and parameter SA algorithms. In this study we used MAAT (tag: v1.2.1_walkeretal2020_GCB, commit hash: 09b1479).

2.1 | Additional model details

Figure 1 shows a dependency diagram of the general C3 photosynthesis model. Parameters, state parameters (variables that are calculated during model execution but are not the main model state), state variables (i.e. carbon assimilation rate) and their dependencies are shown categorized by the four processes: limiting-rate selection, electron transport, TPU and carboxylation. Each process is composed of multiple parameters and, excepting carboxylation, multiple ways in which they can be represented. Some processes have more than one mathematical function in their representation, e.g. carboxylation which includes Equations (1), (4), (5) and (8).

Note that in the original studies, FvCB and CBGB describe the enzyme-kinetic models using different units and slightly different parameter definitions. In this study we use the unification of
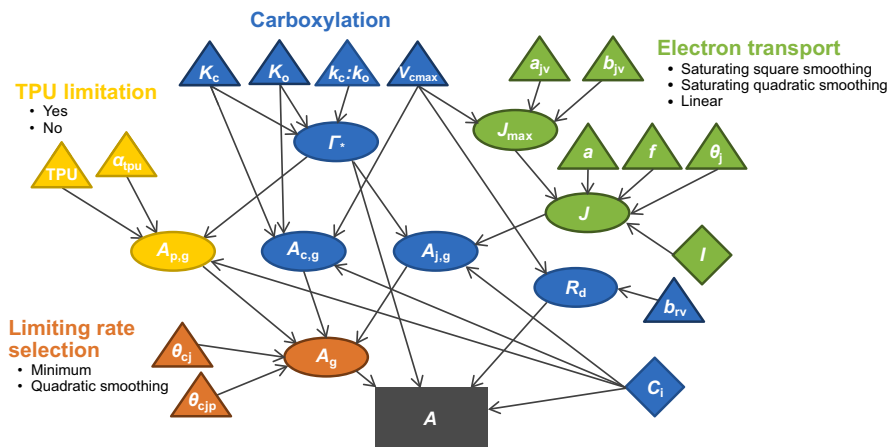
FIGURE 1 Diagram of photosynthesis model to calculate net carbon assimilation (A, μmol m^{-2} s^{-1}, grey rectangle). Inputs (diamonds), parameters (triangles), functions (ellipses) and target state variable (rectangle) are shown, as is the breakdown on the model into the four processes (colours; limiting-rate selection, carboxylation, electron transport and triose phosphate use). Arrows represent the flow of information from distal parts of the model (inputs and parameters), through intermediate functions to the end goal. Concept modified slightly from Coon et al. (2016)

definitions and units presented in Walker et al. (2018) that are built upon Gu et al. (2010) and predominantly follow FvCB. Building on the model details presented in the introduction, Γ_* can be simulated as a function of K_c and K_o:

$$\Gamma_* = \frac{k_o K_c O_i}{2 k_c K_o},\tag{8}$$

where k_o and k_c are the turnover numbers for the oxygenase and carboxylase functions of RuBisCO. At 25°C k_o is 0.21 times k_c, and their activation energies are the same so this ratio is preserved across a range of temperatures (Farquhar et al., 1980).

J_{max} can be represented in a number of ways but many studies have demonstrated the tight correlation between J_{max} and V_{cmax} (Leuning et al., 1995; Walker, Beckerman, et al., 2014; Wullschleger, 1993) and for the basis of this study we use the commonly employed linear relationship based on the relationship proposed by (Wullschleger, 1993):

$$J_{max,25} = a_{jv} + b_{jv} V_{cmax,25},\tag{9}$$

where a_{jv} and b_{jv} are calculated from linear regression of $J_{max,25}$ on $V_{cmax,25}$ (which are J_{max} and V_{cmax} at a reference temperature of 25°C). We use a similar relationship to calculate TPU:

$$TPU_{25} = b_{tv} V_{cmax,25}.\tag{10}$$

We focus on the core components of the FvCB and CBGB models and do not consider choices of CO_2-diffusion resistance models (i.e. leaf boundary layer, stomata and internal; see Collatz et al., 1991; Walker et al., 2018) nor temperature response models, which would substantially increase scope. Further, while stomatal models do influence C_i, the response to I and C_a of many stomatal models used by TBMs is similar, i.e. $g_s = f(A/C_a)$. In order to preserve realism in the calculation of A we used the unified stomatal model (Medlyn et al., 2011) with a g_1 of 4.3, the global C3 mean (Lin et al., 2015), and a typical value of 0.01 mol m^{-2} s^{-1} for g_0. We assume that leaf internal resistance and leaf boundary layer resistance are 0, vapour pressure deficit is 1 kPa, and no soil water limitation. Leaf temperature was set to a standard of 25°C (which assumes that all temperature sensitive parameters were at 25°C reference values).

To generate C_a and I response curves, the two models were run from a C_a of 50–1,500 μmol/mol in 50 μmol/mol increments at I of 960 μmol m^{-2} s^{-1}, and from I of 10–1,960 μmol m^{-2} s^{-1} in increments of 50 μmol m^{-2} s^{-1} at C_a of 400 μmol/mol.

2.2 | Sensitivity analysis

We use statistical, variance-based process SA and parameter SA which both rely on an ensemble of model simulations to calculate model output variance and ascribe this variance to variation in processes and parameters. The photosynthesis model process SA was broken into four processes: limiting-rate selection (two

representations, Equations 2 or 3), electron transport (three representations, Equations 6a–c), TPU limitation (included or not included, Equation 7) and carboxylation (one representation, Equation 4). Factorial combination of the alternative process representations gives a total of 12 individual models. For both the process SA and parameter SA, 14 parameters were varied ±10% from a central, commonly used value (Table 2). Thus the model ensemble comprises 12 individual models and variation of 14 parameters.

Both methods calculate sensitivity indexes that represent the proportion of variance in model-ensemble output (both between and within-model variance for the process SA, and just within-model variance for the parameter SA) caused by variance in either a specific process or a specific parameter. Process SA provides a quantitative assessment of the influence of processes on model output and includes both variation caused by alternative hypotheses for the mechanics of a given process, and variation caused by parameters within a given process, i.e. between-model and within-model variability (Dai et al., 2017). Parameter SA can assess the influence of individual parameters on within-model variance. The parameter SA method does not account for variance caused by the different central tendencies (means) of each model combination. For process SA the algorithm of Dai et al. (2017) was used and for parameter SA the algorithm of Saltelli et al. (2010) was used (see Walker et al., 2018 for additional description of both methods).

In this analysis we calculate and focus on first order sensitivity indexes, analogous to main effects in ANOVA. We do not calculate two-way or higher order interactions among processes or parameters. While some interactions are likely to be interesting, the sum of first order sensitivity indexes sum to around 0.95 in many cases indicating that over 95% of variance in model output was explained by first order effects.

For both analyses, we investigated sensitivities of simulated carbon assimilation (A, Equation 1) across a number of environmental scenarios that were a factorial combination of atmospheric CO_2 (C_a; 280, 400 and 600 μmol/mol) and incident light (I; 200, 500, and 1,000 μmol photons m^{-2} s^{-1}) conditions. The sensitivity of the absolute assimilation response (ΔA) to changes in C_a (from preindustrial to present-day, 280–400 μmol/mol, and from present-day to projected future concentrations, 400–600 μmol/mol) were also calculated under the three incident light conditions. Variance-weighted means of the sensitivity indexes across different environment combinations allow us to quantify the general influence of a process or parameters across environment combinations. For parameters this can also be done across model combinations, but again still only account for within model variance.

Parameter samples were drawn from uniform distributions and were multi-dimensional (all parameters varied together) but no covariance among parameters was assumed. CBGB used values of 0.95 and 0.98 for θ_{cj} and θ_{cjp}, see table A1 in CBGB. Note values are switched in the text of CBGB, i.e. 0.98 and 0.95 for θ_{cj} and θ_{cjp}. Other values have since been used by TBMs; e.g. 0.9 in IBIS (Foley et al., 1996) and 0.83 in JULES (Clark et al., 2011). The possible values for these smoothing parameters are from $0 \le \theta \le 1$ and so to

TABLE 2 Comparison of the parameters used in the original papers by Farquhar and Collatz unified to common units

Parameter	Equations	Description	Units	FvCB	CBGB	SA range
V_{cmax}	4, 9 and 10	Maximum RuBisCO carboxylation rate	$\mu mol\ CO_2\ m^{-2}\ s^{-1}$	98	200	45–55
K_c	4 and 8	Michaelis–Menten constant of RuBisCO for CO_2	Pa	46	30	36.4–44.5
K_o	4 and 8	Michaelis–Menten constant of RuBisCO for O_2	kPa	33	30	25.1–30.6
$k_o{:}k_c$	8	Ratio of RuBisCO turnover numbers for O_2 and CO_2	—	0.21	0.38[a]	0.19–0.23
J_{max}	6a, 6b and 9	Maximum electron transport rate	$\mu mol\ e\ m^{-2}\ s^{-1}$	210	na	na
a_{jv}	9	Intercept of J_{max} to V_{cmax} relationship	$\mu mol\ e\ m^{-2}\ s^{-1}$	na	na	26.2–32.0
b_{jv}	9	Slope of J_{max} to V_{cmax} relationship	$e\ CO_2^{-1}$	na	na	1.467–1.804
a	6	Leaf absorbtance of visible solar radiation	—	na (0.80)[b]	0.86	0.72–0.88
$f\ (\alpha_i = 1 - f)$	6	Fraction of absorbed light not absorbed by photosystems	—	0.23	0.52[c]	0.207–0.253
θ_j	6a	Electron transport smoothing	—	na (0.67)[b]	na	0.81–0.99
θ_{cj}	3a	Assimilation rate smoothing 1	—	na	0.95	0.81–0.99
θ_{cjp}	3b	Assimilation rate smoothing 2	—	na	0.98	0.81–0.99
TPU	7	Triose phosphate utilisation	$\mu mol\ CO_2\ m^{-2}\ s^{-1}$	na	$0.167\ V_{cmax}$	$0.15–0.183\ V_{cmax}$
α_{tpu}	7	Fraction of phosphate exported from chloroplast not returned	—	na	na	0.45–0.55
R_d	1	Dark respiration	$\mu mol\ CO_2\ m^{-2}\ s^{-1}$	1.1	$0.015\ V_{cmax}$	$0.0135–0.0165\ V_{cmax}$

Abbreviation: TPU, triose phosphate use.

[a]Calculated from Collatz $CO_2{:}O_2$ specificity ratio, τ in their notation, of 2,600 where $k_o{:}k_c = K_o/(K_c\tau)$.

[b]Parameters were not originally specified in Farquhar but values in parentheses featured in Farquhar and Wong (1984).

[c]Calculated from Collatz value of intrinsic quantum yield, α in their notation, of 0.08 where $0.5(1 - f)/4 = \alpha$.

maintain values within this range and preserve the ±10% variation in all parameters, we use a central value of 0.9 for θ_{cj} and θ_{cjp}. These data are publically available (Walker, Lu, et al., 2020).

To assess convergence in sensitivity index calculations, preliminary SAs were run with an n of 1,000 for the process SA and 1,000,000 for the parameter SA. Subsampling and bootstrapping indicated that an n of 300 for the process SA and 300,000 for the parameter SA were ample to achieve convergence (standard deviations of the sensitivity indexes were less than 0.001). The results of the SA shown in this study were generated using these smaller values of n, resulting in a total of 4,320,000 executions for the process SA and 50,400,000 for the parameter SA. These total number of executions are larger than n as n is the base number of samples and the full SAs require multiple sets of iterations that are a function of the number of model combinations and parameters investigated (see Walker et al., 2018).

2.3 | Estimation of θ_{cj} from high-resolution A–C_i curves

High-resolution A–C_i curves (Anderson et al., 2020) were used to evaluate limiting-rate selection hypotheses. *Populus canadensis*

Moench. [deltoides × nigra] clone OP367 was grown outside at Brookhaven National Laboratory, NY, USA in 200 L pots containing 52 Mix (Conrad Fafard, Inc.). Hardwood cuttings were planted on 1 May 2019 and plants were watered to field capacity two to three times a week. Photosynthetic CO_2 response (A–C_i) curves were measured using a LI-6800 Portable Photosynthesis System (LI-COR) in June 2019.

Preliminary measurements identified saturating I and C_a where photosynthesis transitioned from RuBP saturated ($A_{c,g}$) to RuBP limited ($A_{j,g}$) photosynthesis. These preliminary measurements informed a commonly used A–C_i response protocol (Rogers, Serbin, et al., 2017), developed to include a high density of measurements around the transition point (when $A_{c,g} = A_{j,g}$). Leaves were first acclimated to chamber conditions ($I = 2,000\ \mu mol\ m^{-2}\ s^{-1}$, $C_a = 400\ \mu mol/mol$, flow rate = 600 μmol/s, relative humidity = 70%–75%, leaf temperature = 30°C) and measurements began once steady-state gas exchange was achieved. C_a was taken from 400 to 50 μmol/mol then returned to a conservative estimate of the start of the transition zone (305 μmol/mol) and raised progressively in 5 μmol/mol increments to 1,000 μmol/mol (a value comfortably higher than the end of the transition zone). C_a was then raised in larger increments to capture the full extent of a standard A–C_i curve.

Bayesian machine-learning, Markov chain Monte Carlo (MCMC), algorithms were used to numerically approximate the posterior distribution of the smoothing parameter, θ_{cj} (Equation 3a), and V_{cmax} and J_{max}, from these high-resolution A–C_i curves. Numerical approximation is achieved by randomly sampling from a specified prior distribution, stochastically generating a proposal for the parameters to be estimated, evaluating the likelihood of the proposed parameter values against observed data and iterating the generation of new proposals to search the prior parameter space until convergence of the joint posterior distribution is reached. MCMC algorithms are then further iterated postconvergence to sample the joint posterior distribution. For this analysis, the Differential Evolution Adaptive Metropolis (DREAM) algorithm (Vrugt et al., 2009) was chosen due to its efficient search of parameter space and rapid convergence relative to other MCMC algorithms.

The DREAM algorithm optimizes parameter space sampling in several ways (Vrugt, 2016). First, the algorithm employs multiple parallel MCMC chains and parameter proposals are generated from randomly selected chain pairs. A scaling factor is used to scale the 'jump' distance of the new proposal from the previously accepted proposal. At approximately every fifth iteration the scaling factor is set to 1 to avoid convergence in local minima. The algorithm avoids the inefficiency that arises from updating all parameters of a chain simultaneously by updating only a randomly selected subset (the 'crossover') of the parameters on a chain with optimized probability. Outlier chains are identified based on the interquartile range of the posterior likelihood and replaced with the sample history of another randomly chosen non-outlier chain.

Coded within the MAAT software framework, the DREAM algorithm used the high-resolution A–C_i data to formally estimate the parameter values for $V_{cmax,25}$, $J_{max,25}$, and θ_{cj} for each leaf. Uniform priors were used, taking the values 100–200 μmol CO_2 m^{-2} s^{-1} for $V_{cmax,25}$, 70–400 μmol e m^{-2} s^{-1} for $J_{max,25}$, and 0.9–1.0 for θ_{cj} (unitless). Environmental variables were set to the conditions used to generate the A–C_i curves (see above). Given the high rates of photosynthesis in these plants, temperature optima of V_{cmax} and J_{max} were assumed high at 35 and 30°C. Seven Markov chains were run for 80,000 iterations. The standard error probability density function with independent and identically distributed (iid) error residuals was used to compute the log-likelihood of the proposal generation. On completion of the 80,000 iterations convergence was determined using the Gelman and Rubin (1992) R-statistic. Preconvergence samples were discarded yielding 25,000 postconvergence samples on each chain, these were then thinned to 1% to remove auto-correlation.

2.4 | TBM simulations

We use three TBMs to test the impact of quadratic smoothing on global GPP simulations: (a) the Energy Exascale Earth System Model (E3SM) land model (ELM; release: v1.1.0; Burrows et al., 2020), a coupled carbon, nitrogen and phosphorus model with sun/shade big-leaf canopy photosynthesis scaling. (b) The Functionally Assembled Terrestrial Ecosystem Simulator (FATES, tag: sci.1.30.0_api.8.0.0; Koven et al., 2019), coupled with the Community Land Model (CLM, version 5; Lawrence et al., 2019), a carbon-only vegetation demography model with multi-leaf and multi-canopy layers for scaling photosynthesis, and with a leaf area index (LAI) optimization scheme. (c) The Sheffield Dynamic Global Vegetation Model (SDGVM, tag: Walkeretal2020_GCB), a carbon-only model with multi-leaf-layer canopy photosynthesis scaling and also with an LAI optimisation scheme (Walker et al., 2017; Woodward & Lomas, 2004). The leaf photosynthesis model in both ELM and FATES is based on CBGB but with an electron transport function that includes a J_{max} term (Equation 3a). While SDGVM uses the FvCB model with a similar electron transport function (Equation 3b). For more information about the models, see Notes S1.

Models were run each using their common configurations and input datasets to allow for a cross-section of results. The goal was to assess the possible impacts of smoothing in global TBM simulations across a range of model types rather than to quantify the exact impact under a specific set of conditions. Thus, commonly used configurations allowed a broader sampling of the possible model configuration space. The only strict protocol was to use consistent values for the smoothing parameters. Two simulations were conducted: a simulation using smoothing parameters (0.95 for θ_{cj} and 0.98 for θ_{cjp}) and a no-smoothing simulation in which the minimum of limiting rates were taken or where smoothing was effectively disabled by setting their parameter values to 1 or 0.9999 (for both). Decadal average annual GPP from the two simulations were then compared to determine the impact of the smoothing parameters. Model results were re-gridded to a common 0.5° × 0.5° spatial grid, using bilinear interpolation where necessary (ELM). A 0.5° land mask was then applied to constrain model output to a common areal extent on which to base annual calculations and maps of global GPP (Walker, Fisher, et al., 2020).

3 | RESULTS

In their original parameterizations, the C_a response of CBGB is smoother and more sensitive than FvCB at both low and high C_a (Figure 2a). With unified parameters the models are similar at low to intermediate C_a but at high C_a the CBGB model is again more sensitive to C_a and the difference in A approaches 10 μmol m^{-2} s^{-1} at 1,500 μmol/mol (Figure 2b). Comparison of A implied by each of the two or three potentially limiting rates (i.e. calculating A from $A_{c,g}$, $A_{j,g}$, and $A_{p,g}$ in Equation 1) explains these responses (Figure 2c,d).

A in the FvCB model tracks exactly A implied by one of the two potentially limiting rates and consequently shows a sharp transition at the point where carboxylation-limited and light-limited rates are equal (Figure 2c). Above this transition point light limits A, though some sensitivity to C_a remains due to competitive-inhibition of photorespiration. For the CBGB model, A also closely tracks the carboxylation-limited rate at low C_a. Between 300 and 400 μmol/mol A begins to deviate from any A implied by the three potentially limiting

FIGURE 2 Comparison of FvCB (solid black line) and CBGB (dashed black line) calculated carbon assimilation (A, µmol m^{-2} s^{-1}) in response to C_a (left column) and I (right column) for the models, (a) and (e) in their original state and parameterization (Table 1), (b) and (f) in their original state but with common parameterization (using FvCB parameters Table 1). (c and g) FvCB and (d and h) CBGB showing the two or three potentially limiting rates $A_{c,g}$ (green), $A_{j,g}$ (blue) and $A_{p,g}$ (purple) in addition to A (black solid or dashed). Vertical grey lines show the transition points between limiting rates for the FvCB (solid) and CBGB (dashed) models. Common parameterizations are for shared parameters, i.e. the quadratic smoothing parameters are not common as quadratic smoothing is not considered by FvCB even though selection of the minimum can be represented by a special case of quadratic smoothing
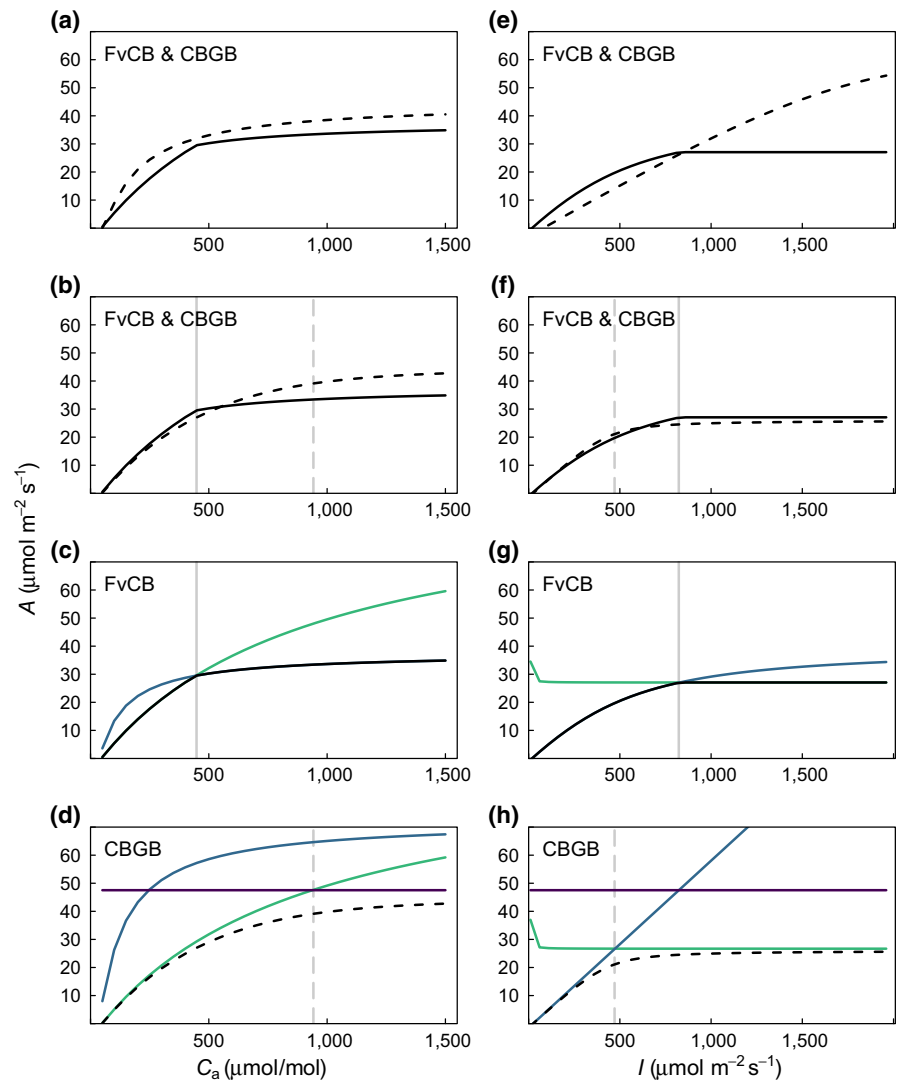
rates (Figure 2d); a consequence of quadratic smoothing (Equations 3a,b). The largest departure of A from any of the implied rates (a difference close to 10 µmol m^{-2} s^{-1}) is at the transition point which, notably, is between the carboxylation-limited rate and the TPU-limited rate, not the light-limited rate. The light-limited rate is much greater than A, by over 20 µmol m^{-2} s^{-1} for most of the range in C_a concentrations (Figure 2d). Thus the continued sensitivity of A to C_a above the transition point results not from suppression of photorespiration, but from less influence of quadratic smoothing as TPU limitation becomes the dominant limiting rate (reduction of A by smoothing increases as limiting rates become more similar, discussed in more detail below).

With their original parameterizations the light responses of the two models are very different (Figure 2e). The FvCB model shows a curve similar in nature to its C_a response, a steep increase, an abrupt transition followed by saturation; while the CBGB model shows a close to linear increase across the range of I. The linear response to I of CBGB results from the (a) very high V_{cmax} (200 µmol m^{-2} s^{-1}, Table 2) in the original parameterization, which prevents C_a limitation at 400 µmol/mol across the range of I, and (b) the absence of a J_{max} term in the electron

transport response (Equation 6c) which therefore hypothesizes a linear response of electron transport to I. At common parameter values (Figure 2f), the curves are much more similar. This is because at the lower, common V_{cmax} (98 µmol m^{-2} s^{-1}) A_c becomes limiting at 400 µmol/mol. For light, A in both models tracks A implied by the potentially limiting rates more closely than for CO_2 (Figure 2g,h). This is because the transition between the implied rates is more abrupt and therefore the range of I where smoothing occurs is narrower. The greatest difference among the two models are in their light-limited rates, FvCB shows strong non-linearity and saturates (due to the J_{max} term in Equation 6a) while CBGB shows a linear response to light (Equation 6). Curvature in the light response of realised assimilation rates come from the θ_j parameter for the FvCB model and the θ_{cj} parameter for the CBGB model.

3.1 | SA of assimilation (A)

Figure 3a shows distributions of A when varying representations of the three processes and the values of the 14 parameters (Table 3)
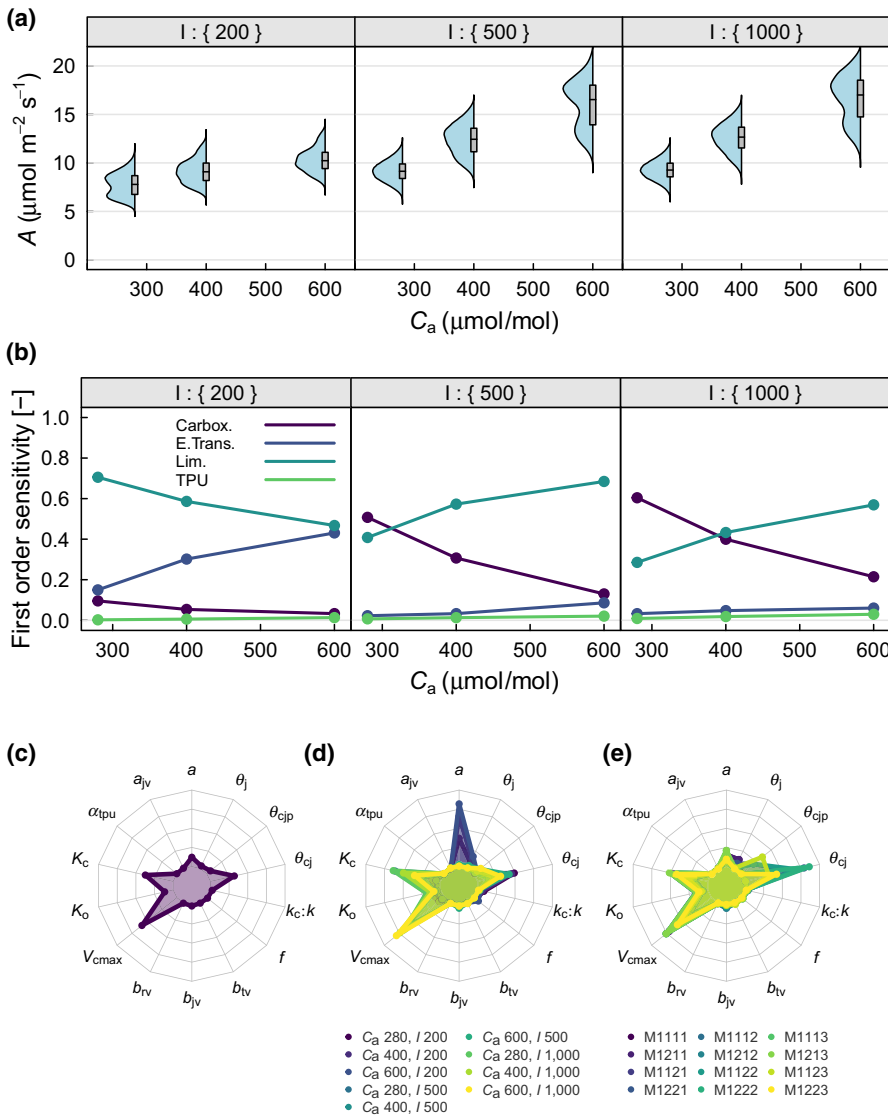
FIGURE 3 Sensitivity of carbon assimilation (A, µmol m^{-2} s^{-1}) to variability in processes and parameters across various C_a and I environmental conditions. (a) Semi violin plots showing distributions of A against C_a (µmol/mol, x-axis) and I (µmol m^{-2} s^{-1}, panels) boxes represent the interquartile range and median, whiskers the full range. (b) First order sensitivity index of A to variability in the four processes against C_a (µmol/mol, x-axis) and I (µmol m^{-2} s^{-1}, panels). (c) First order sensitivity index of A to variability in the 14 parameters, indexes integrated across the 12 models and nine environmental conditions. (d) First order sensitivity index of A to variability in the 14 parameters, indexes integrated across the 12 models and colour coded for each of the nine environmental conditions. (e) First order sensitivity index of A to variability in the 14 parameters, indexes integrated across the nine environmental conditions and colour coded for each of the 12 models

across nine combinations of C_a and I (i.e. different environmental conditions). As C_a increases, A and variance of A increases (Figure 2a; Table 1). Distributions are primarily unimodal, though several bimodal distributions are apparent.

Across all environmental conditions, limiting-rate selection was responsible for 57% of the variation in A, carboxylation responsible for 22%, electron transport 10% and TPU 2% (Table 3). The strong influence of limiting-rate selection was borne out across the majority of environmental conditions (Figure 3b). However, at saturating I (1,000 µmol m^{-2} s^{-1}) the process of carboxylation was most influential at preindustrial C_a (280 µmol/mol), and at present-day C_a (400 µmol/mol) the influence of carboxylation was about equal to limiting-rate selection. This pattern was similar at close to saturating I (500 µmol m^{-2} s^{-1}), but limiting-rate selection had a generally higher influence. At low values of I (200 µmol m^{-2} s^{-1}), the process of electron transport was more influential than carboxylation with the sensitivity of A to electron transport increasing as C_a becomes less limiting. Bimodality was most apparent when limiting-rate selection was most influential (the alternative modes

corresponding with the two alternative representations of limiting-rate selection).

When all 12 models and all nine environmental scenarios were combined, variation in A of more than 5% was caused by only five of the 14 parameters (Figure 3c; Table 4). V_{cmax} was the most influential parameter responsible for 35% of the variation in A, followed by K_c with 22%, θ_{cj} with 19%, K_o with 7%, and a with 7%.

The influence of these parameters somewhat reflects the influence of the processes to which they belong. However, if we were to only consider variability in A caused by parameter variation, the influence of carboxylation would be over-estimated. V_{cmax}, K_o and K_c are all parameters in the process of carboxylation and together they were responsible for 64% of the variation in A in the parameter SA (total variance: 0.94). Together θ_{cj} and θ_{cjp}, the parameters of limiting-rate selection, were responsible for only 23% of variance in the parameter SA. On the other hand, the process SA suggested that carboxylation was responsible for a more modest 22% of the variation in A (total variance: 2.59), while limiting-rate selection was responsible for 57%. The results

TABLE 3 First order sensitivity to processes

Variable	C_a	I	Mean	Variance	Carbox.	E.Trans.	Lim.	TPU
A	int[a]	int	11.49	2.59	0.22	0.10	0.57	0.02
	280	200	7.77	1.46	0.10	0.15	0.71	0.00
	400	200	9.15	1.54	0.05	0.03	0.59	0.01
	600	200	10.31	1.49	0.03	0.43	0.47	0.01
	280	500	9.16	1.11	0.51	0.02	0.41	0.01
	400	500	12.38	2.61	0.31	0.03	0.57	0.01
	600	500	16.08	6.19	0.13	0.09	0.68	0.02
	280	1,000	9.28	0.99	0.60	0.03	0.29	0.01
	400	1,000	12.61	2.21	0.40	0.05	0.43	0.02
	600	1,000	16.68	5.76	0.21	0.06	0.57	0.03
ΔA	int	int	2.81	0.50	0.05	0.13	0.65	0.03
	280–400[b]	200	1.38	0.10	0.10	0.50	0.07	0.01
	400–600	200	1.16	0.04	0.11	0.32	0.37	0.05
	280–400	500	3.22	0.40	0.07	0.05	0.76	0.02
	400–600	500	3.70	1.11	0.02	0.18	0.64	0.03
	280–400	1,000	3.32	0.32	0.11	0.07	0.64	0.04
	400–600	1,000	4.07	1.02	0.05	0.07	0.69	0.04

Abbreviation: TPU, triose phosphate use.

[a]Integrated across environmental scenarios.

[b]For a change in Ca from 280 to 400 μmol/mol.

presented here suggest that variation in A between the alternative limiting-rate selection models (hypotheses) was substantial, and not solely a result of variation in parameters. The difference in variance accounting by the two methods is demonstrated by the difference in variance calculated by the parametric SA (0.94) and the process SA (2.59) despite both algorithms using all possible model combinations and the same parameter ranges (the means of A calculated by the algorithms were equivalent: 11.49 and 11.49; Tables 3 and 4).

Sensitivities for individual models (integrated across environmental scenarios) showed that, given equal variation (±10%), V_{cmax} and θ_{cj} shared similar maximum sensitivities: 48% and 52% respectively (Figure 3e; Table 4). θ_{cjp} had a maximum sensitivity of 21% in the model with smoothing, TPU and no J_{max} term in electron transport (M1223). Leaf light absorption, a, featured in all models of electron transport, and therefore all models, and sensitivity to a varied between 9% and 13% or 3%–6% depending on minimum or smoothing limiting-rate selection respectively. Similarly, V_{cmax}, K_o and K_c were all more influential in the models that used the minimum for limiting-rate selection. Sensitivities for individual environmental conditions (integrated across models) showed that as expected a was influential under low-light conditions while V_{cmax}, K_o and K_c were influential under high-light conditions (Figure 3d). Sensitivities for individual model and environmental condition combinations showed that for some cases some of the previously unmentioned parameters were influential (e.g. θ_j, f), while others remained with very little influence (e.g. a_{jv}, b_{jv}, b_{tv}, α_{TPU}).

3.2 | SA of the assimilation response (ΔA) to changes in C_a

Figure 4a shows the distribution of ΔA in response to changes in C_a (from preindustrial to present-day, 280–400 μmol/mol, and from present-day to projected future concentrations, 400–600 μmol/mol) at three levels of I. Variation of ΔA was greatest at intermediate light levels and going from present to future C_a (range about 2 to 5 μmol m^{-2} s^{-1}). Variation was similar at high light. For both C_a changes and at both high and intermediate light, the distribution of ΔA was highly bimodal, with stronger bimodality going from preset to future C_a. As for A, the alternative modes were associated with the alternative representations of limiting-rate selection.

When all environmental scenarios were combined, limiting-rate selection was responsible for 65% of the variation in ΔA (total variance: 0.50), carboxylation responsible for 5%, electron transport 13% and TPU 3% (Table 3). The strong influence of limiting-rate selection was borne out across the majority of environmental conditions (Figure 4b). For both C_a changes and at high and intermediate I, sensitivity of ΔA to limiting-rate selection ranged from 64% to 76%, with the higher sensitivities at intermediate I. At low I electron transport was the most influential process, accounting for 50% of the variation in ΔA at the lower C_a change and 32% at the higher C_a change. At low I sensitivity of ΔA to limiting-rate selection increased from 7% at the lower C_a to 37% at the higher C_a.

In contrast with the sensitivity of A, seven parameters were responsible for over 5% variation in ΔA (total variance−0.09) when models and environmental scenarios were combined. Of these seven

TABLE 4 First order sensitivity to parameters

Variable	C_a	I	Model	Mean	Variance	a	a_{jv}	α_{tpu}	K_c	K_o	V_{cmax}	b_{jv}	b_{rv}	b_{tv}	f	$k_c{:}k_o$	θ_{cj}	θ_{cjp}	θ_j
A	int	int	int	11.49	0.94	0.07	0.00	0.00	0.22	0.07	0.35	0.00	0.01	0.00	0.01	0.01	0.19	0.04	0.02
	280	200	int	7.77	0.44	0.22	0.00	0.00	0.16	0.09	0.05	0.00	0.00	0.00	0.02	0.05	0.29	0.00	0.05
	400	200	int	9.14	0.52	0.39	0.00	0.00	0.07	0.05	0.02	0.00	0.00	0.00	0.03	0.04	0.27	0.01	0.08
	600	200	int	10.30	0.55	0.49	0.00	0.00	0.03	0.03	0.02	0.00	0.00	0.00	0.04	0.02	0.21	0.03	0.10
	280	500	int	9.15	0.69	0.00	0.00	0.00	0.36	0.11	0.37	0.00	0.00	0.00	0.00	0.02	0.13	0.01	0.00
	400	500	int	12.37	1.11	0.00	0.00	0.00	0.28	0.08	0.41	0.00	0.00	0.00	0.00	0.01	0.19	0.03	0.01
	600	500	int	16.07	1.52	0.02	0.00	0.00	0.15	0.05	0.38	0.00	0.03	0.00	0.00	0.01	0.25	0.06	0.03
	280	1,000	int	9.28	0.69	0.00	0.00	0.00	0.38	0.11	0.39	0.00	0.00	0.00	0.00	0.02	0.09	0.01	0.00
	400	1,000	int	12.61	1.12	0.00	0.00	0.00	0.30	0.08	0.44	0.00	0.01	0.00	0.00	0.01	0.14	0.03	0.00
	600	1,000	int	16.67	1.80	0.00	0.00	0.00	0.21	0.05	0.48	0.00	0.01	0.01	0.00	0.01	0.18	0.07	0.00
	int	int	1111	12.47	0.96	0.09	0.00	0.00	0.28	0.09	0.42	0.00	0.01	0.00	0.01	0.02	0.00	0.00	0.08
	int	int	1211	12.47	0.96	0.09	0.00	0.00	0.28	0.09	0.42	0.00	0.01	0.00	0.01	0.02	0.00	0.00	0.08
	int	int	1121	9.82	0.92	0.04	0.00	0.00	0.11	0.04	0.23	0.00	0.01	0.00	0.00	0.01	0.39	0.12	0.04
	int	int	1221	10.47	1.07	0.03	0.00	0.00	0.13	0.04	0.22	0.00	0.01	0.00	0.00	0.01	0.47	0.00	0.04
	int	int	1112	12.28	0.82	0.09	0.01	0.00	0.30	0.10	0.45	0.01	0.03	0.00	0.01	0.02	0.00	0.00	0.00
	int	int	1212	12.28	0.82	0.09	0.01	0.00	0.30	0.10	0.45	0.01	0.03	0.00	0.01	0.02	0.00	0.00	0.00
	int	int	1122	9.65	0.84	0.03	0.00	0.00	0.11	0.04	0.23	0.00	0.01	0.00	0.00	0.01	0.42	0.12	0.00
	int	int	1222	10.27	0.97	0.03	0.00	0.00	0.13	0.04	0.22	0.00	0.01	0.00	0.00	0.01	0.52	0.00	0.00
	int	int	1113	12.82	1.00	0.13	0.00	0.00	0.31	0.09	0.45	0.01	0.00	0.00	0.01	0.02	0.00	0.00	0.00
	int	int	1213	12.82	1.00	0.13	0.00	0.00	0.31	0.09	0.45	0.01	0.00	0.00	0.01	0.02	0.00	0.00	0.00
	int	int	1123	10.80	0.93	0.05	0.00	0.00	0.17	0.05	0.31	0.01	0.00	0.01	0.01	0.01	0.19	0.21	0.00
	int	int	1223	11.67	0.97	0.06	0.00	0.00	0.25	0.07	0.34	0.00	0.00	0.00	0.00	0.01	0.25	0.00	0.00
ΔA	int	int	int	2.81	0.09	0.09	0.01	0.00	0.09	0.02	0.26	0.00	0.07	0.01	0.01	0.00	0.20	0.11	0.05
	280–400	200	int	1.38	0.07	0.38	0.00	0.00	0.11	0.03	0.17	0.00	0.01	0.00	0.04	0.01	0.02	0.02	0.05
	400–600	200	int	1.16	0.02	0.34	0.00	0.00	0.15	0.09	0.02	0.00	0.01	0.00	0.03	0.07	0.09	0.10	0.07
	280–400	500	int	3.22	0.07	0.01	0.00	0.00	0.07	0.01	0.41	0.00	0.01	0.00	0.00	0.00	0.36	0.10	0.02
	400–600	500	int	3.70	0.21	0.07	0.01	0.00	0.11	0.01	0.10	0.00	0.15	0.00	0.00	0.00	0.13	0.08	0.10
	280–400	1,000	int	3.32	0.07	0.00	0.00	0.00	0.08	0.01	0.47	0.00	0.02	0.01	0.00	0.00	0.30	0.13	0.01
	400–600	1,000	int	4.07	0.12	0.01	0.01	0.00	0.04	0.01	0.42	0.00	0.03	0.02	0.00	0.01	0.27	0.21	0.01
	int	int	1111	3.20	0.10	0.04	0.00	0.00	0.08	0.01	0.29	0.00	0.06	0.00	0.00	0.00	0.00	0.00	0.20
	int	int	1211	3.20	0.10	0.04	0.00	0.00	0.08	0.01	0.29	0.00	0.06	0.00	0.00	0.00	0.00	0.00	0.20
	int	int	1121	2.05	0.09	0.03	0.01	0.00	0.04	0.02	0.08	0.00	0.03	0.02	0.01	0.01	0.33	0.36	0.07

(Continues)

TABLE 4 (Continued)

Variable	C_a	I	Model	Mean	Variance	a	a_{jv}	α_{tpu}	K_c	K_o	V_{cmax}	b_{jv}	b_{rv}	b_{tv}	f	$k_c{:}k_o$	θ_{cj}	θ_{cjp}	θ_j
	int	int	1221	2.44	0.10	0.03	0.00	0.00	0.01	0.00	0.09	0.00	0.04	0.00	0.00	0.00	0.65	0.00	0.11
	int	int	1112	3.10	0.11	0.11	0.03	0.00	0.20	0.02	0.29	0.00	0.21	0.00	0.01	0.01	0.00	0.00	0.00
	int	int	1212	3.10	0.11	0.11	0.03	0.00	0.20	0.02	0.29	0.00	0.21	0.00	0.01	0.01	0.00	0.00	0.00
	int	int	1122	1.98	0.07	0.03	0.01	0.00	0.05	0.02	0.08	0.00	0.04	0.02	0.01	0.01	0.36	0.38	0.00
	int	int	1222	2.35	0.08	0.04	0.00	0.00	0.02	0.00	0.09	0.00	0.05	0.00	0.00	0.00	0.74	0.00	0.00
	int	int	1113	3.33	0.10	0.21	0.01	0.01	0.11	0.03	0.55	0.01	0.01	0.01	0.02	0.01	0.01	0.01	0.01
	int	int	1213	3.33	0.10	0.21	0.01	0.01	0.11	0.03	0.55	0.01	0.01	0.01	0.02	0.01	0.01	0.01	0.01
	int	int	1123	2.53	0.11	0.05	0.01	0.01	0.03	0.02	0.15	0.01	0.01	0.05	0.01	0.01	0.12	0.61	0.01
	int	int	1223	3.11	0.07	0.11	0.00	0.00	0.05	0.00	0.35	0.00	0.00	0.00	0.01	0.00	0.45	0.00	0.00
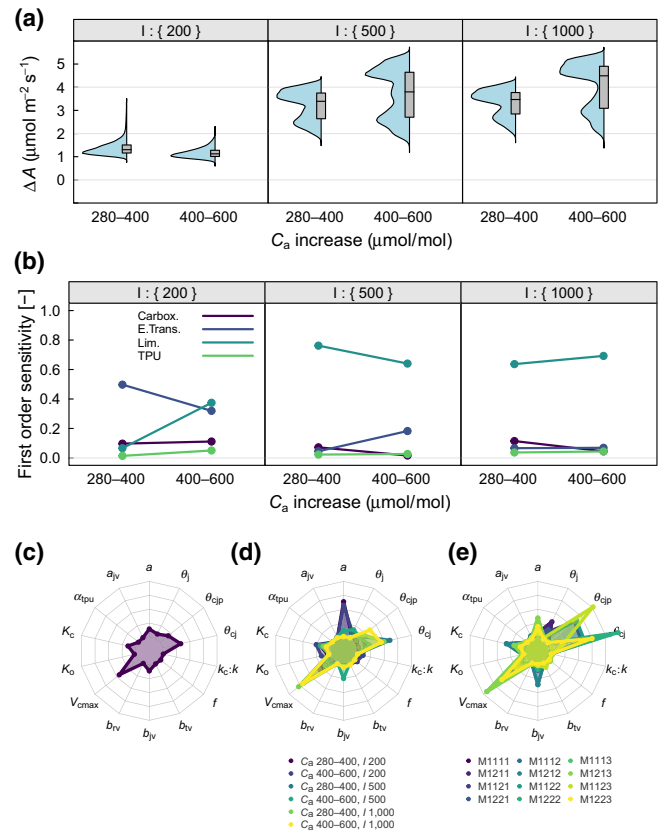
FIGURE 4 Sensitivity of the carbon assimilation response to an increase in C_a (ΔA, µmol m^{-2} s^{-1}) to variability in processes and parameters across I. Descriptions the same as for Figure 3

parameters, four were in common with A (V_{cmax} with 26%, K_c with 9%, θ_{cj} with 20% and a with 9%; Figure 4c; Table 4), K_o did not feature, and θ_{cjp} with 11%, b_{rv} with 7% and θ_j with 5% were also influential.

3.3 | Consequences of limiting-rate selection assumptions

Given the sensitivity of A and ΔA to the processes of limiting-rate selection, we now investigate these models in more detail. Mathematical analysis shows that FvCB sets the upper limit for A while CBGB smoothing always reduces A below that of the minimum (see Supporting Information). The greatest reduction in A caused by smoothing is when all three limiting rates—$A_{c,g}$, $A_{j,g}$ and $A_{p,g}$—are equal, and yields Equation S3 (see Supporting Information). With $\theta_{cj} = 0.95$, $\theta_{cjp} = 0.98$, Equation S3 shows that the smoothing scalar on A_g is 0.77, i.e. when $A_{c,g} = A_{j,g} = A_{p,g}$ quadratic smoothing reduces A_g by 23%. When only $A_{c,g}$ and $A_{j,g}$ are equal and substantially lower than $A_{p,g}$ (so $A_{p,g}$ effectively has no influence on smoothing), A_g is reduced by 18%. Figure 5a shows that A_g is reduced below the minimum rate across a wide range of $A_{c,g}$ and $A_{j,g}$ values and that the reduction in A_g approaches 0 monotonically as the difference between the minimum rate and the larger rate increases.
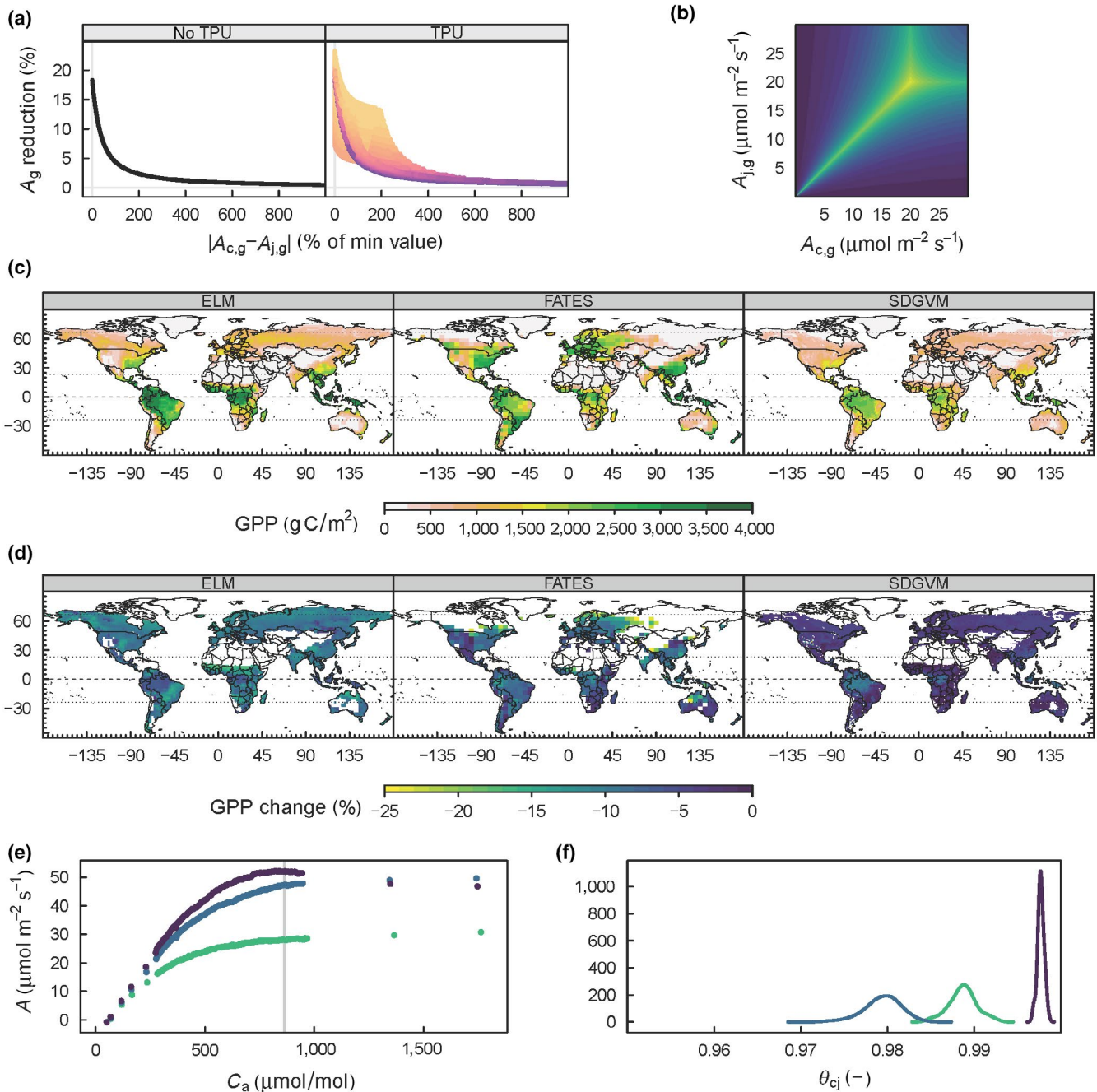
FIGURE 5 Relative reduction in calculated A_g of GPP (%) using quadratic smoothing compared to the minimum of the limiting rates. (a) Relative reduction in A_g (%) against the relative difference in $A_{c,g}$ and $A_{j,g}$ (% increase relative to the minimum of the two rates) when triose phosphate use is not simulated or simulated, colours represent relative difference in $A_{p,g}$ and the minimum of $A_{c,g}$ and $A_{j,g}$ with orange representing the lowest difference and therefore the largest reduction in A_g. (b) The relative reduction in A_g (%) as a function of both $A_{c,g}$ and $A_{j,g}$ when $A_{p,g}$ is 20 μmol m^{-2} s^{-1} (see colour scale for d). (c) Global GPP (g C/m^2) simulated by the three terrestrial biosphere models (TBMs): ELM, FATES and SDGVM. (d) Relative reduction in GPP (%) caused by non-rectangular hyperbolic smoothing in the three TBMs. (e) High-resolution A–C_a curves used to estimate θ_{cj}. (f) MCMC posterior distributions for θ_{cj} estimated from the curves in (e). The vertical grey line in (e) represents the C_a cutoff for the single high-resolution curve that showed a drop in A at high C_a. Where values of GPP in (c) were less than 250 g C/m^2, values in (d) were screened to avoid over-emphasizing high relative changes on small absolute rates of GPP that do not contribute substantially to the global carbon cycle

The results so far are all based on a leaf-scale SA. To investigate the global-scale impact of the most influential leaf-scale processes, a suite of three different TBMs were run with the two alternative versions of limiting-rate selection, and parameter values for smoothing from CBGB (Figure 5c,d). The three models simulate quite different magnitudes and patterns of global GPP (Figure 5c), and in all three models quadratic smoothing reduced global GPP (5.0–16.4 Pg C/year, or 4.4%–9.7%).

3.4 | Discriminating among hypotheses for limiting-rate selection

High-resolution $A–C_i$ curves were taken on three individuals of *Populus canadensis* (Figure 5e) in order to estimate the θ_{cj} parameter, and thus discriminate among the two competing hypotheses for limiting-rate selection. A value close to 1.0 would indicate FvCB and values close to 0.95 or less would indicate CBGB. Bayesian MCMC estimated θ_{cj} for the three curves at 0.98, 0.99 and 0.999 (mean 0.99 ± 0.011 95% CI; Figure 5f). Thus the only data-driven estimate of θ_{cj} made to-date is not significantly different from 1.0, providing support for the FvCB method of limiting-rate selection.

4 | DISCUSSION

A novel, mathematically rigorous, process SA that accounts for both hypothesis (process representation) and parameter variability in common models of photosynthesis has shown that limiting-rate selection was the most influential process, accounting for 57% of variation in A and 65% of variation in ΔA in response to a change in CO_2. For simulating A, carboxylation was the next most influential process (which was all due to parameter variability) followed by electron transport. When simulating ΔA, electron transport was the next most influential process followed by carboxylation. The process of TPU had almost no influence on simulating either A or ΔA under the environmental conditions of this analysis. The substantial influence of the non-mechanistic limiting-rate selection propagates to global simulation of photosynthesis (reducing mean annual global GPP by 5%–10%) and undermines the mechanistic reasoning for including FvCB and CBGB in TBMs. Analysis of novel, high-resolution $A–C_i$ curves provides support for the FvCB method of limiting-rate selection.

4.1 | The influence of limiting-rate selection

Finding the smaller roots of the quadratics described by Equations (3a,b) is intended to smooth the abrupt transition between $A_{c,g}$, $A_{j,g}$ and $A_{p,g}$, and has been described as representing co-limitation between limiting rates. In so doing, smoothing also imposes a reduction of modelled A (Figure 5), reducing A_g by 23% compared with FvCB when all potentially limiting rates are equal and with CBGB parameter values. In models that have chosen to adjust these parameters (e.g. IBIS, JULES; Table 1) the reduction can be even greater. For example, in IBIS the reduction increases to 36% and in JULES to 38% (Equation S3). This scenario, when all potentially limiting rates are equal, results in the greatest smoothing-related reduction in A_g and A, but it is not an extreme physiological scenario. Potential assimilation rates $A_{c,g}$ and $A_{j,g}$ are often observed to be close to co-limiting in saturating light (e.g. Ainsworth et al., 2003; Bernacchi et al., 2005) and the co-ordination hypothesis assumes that $A_{c,g}$ and $A_{j,g}$ are equal under mean environmental conditions (Maire et al., 2012). Co-ordination hypotheses are used in a number of optimization schemes (Smith

et al., 2019; Wang et al., 2017), which maintain photosynthesis close to the transition given a changing environment. If combined with quadratic smoothing, these methods would maximize the influence and reduction of A caused by smoothing, or may have other untoward consequences (e.g. potentially increasing V_{cmax} and hence nitrogen demand).

Until now, the parameter values used in the smoothing function have not been based on data-driven estimates of their values (to the best of our knowledge). We provide initial data-driven estimates of θ_{cj} (0.99 ± 0.011) using high-resolution $A–C_i$ curves, which provide support for the FvCB approach and that smoothing parameters in CBGB and the TBMs which use CBGB are too low. However, the support for the simple FvCB minimum is not definitive, leaving the door open for potential co-limitation. Additional high-resolution $A–C_i$ curves collected across a broad range of species and growth conditions would help determine if estimates of θ_{cj} could be significantly lower than 1, potentially justifying continued inclusion of quadratic smoothing, albeit that the data presented here suggest it would likely be at a lower level than CBGB and the TBMs that currently use quadratic smoothing.

The global-scale reduction in GPP caused by quadratic smoothing, demonstrates that leaf-scale sensitivities propagate through a suite of processes and scales to have global impact in our current generation of TBMs. This propagation of leaf-scale sensitivities holds true across a spectrum of different model assumptions and representations, including: nutrient cycling (ELM), multi-layered canopy scaling (FATES, SDGVM) and competition among PFTs (FATES).

Given that models which include quadratic smoothing have subsequently been evaluated against larger-scale observations (e.g. eddy covariance towers, Bonan et al., 2011), replacing CBGB smoothing with the FvCB minimum could result in a reduction in model skill. Indeed, smoothing, or co-limitation, among potentially limiting photosynthetic rates reduced GPP and therefore improved simulations of global GPP in CLM4 (Bonan et al., 2011). Bonan et al. (2011) used a number of methods to parameterize V_{cmax}, all of which were based on V_{cmax} values estimated using an FvCB type model. As we have shown, and has been previously demonstrated (Johnson & Thornley, 1984), CBGB smoothing reduces A and hence if a CBGB type model had been used to estimate V_{cmax}, V_{cmax} values would have been higher in order to compensate smoothing-related reductions in A. That is to say, estimates of V_{cmax} are not independent of the limiting-rate selection method used in their estimation and that V_{cmax} and θ_{cj} parameter values applied in TBMs should be consistent with the method used to estimate V_{cmax}. For example, IBIS, in comparison with other TBMs has very high values for V_{cmax} (Rogers, 2014) which may have been required during model calibration to compensate for the use of smoothing in limiting-rate selection. In models which tie V_{cmax} to leaf nitrogen and plant nitrogen demand, the implementation of smoothing would have implications for the coupling of carbon and nitrogen cycles by reducing carbon gained per unit leaf nitrogen.

What process is smoothing intended to represent? CBGB introduce smoothing to represent a more realistic transition in the light

response of A, and this could represent imperfect coupling among the cycles of electron transport, carboxylation and photorespiration (Farquhar et al., 1980). It is also possible that smoothing is accounting for different limiting states of individual chloroplasts within a leaf (Buckley et al., 2017; Kull & Kruijt, 1998). For canopy scale big-leaf models, smoothing is also accounting for different limiting states of leaf layers within either the sunlit or shaded canopy fraction. There is also an intermediate scale where smoothing could be accounting for different limiting states of leaves within a canopy leaf layer (also potentially within either the sunlit or shaded fraction). To use a leaf-scale empirical function as a catch-all for all of these processes is not satisfying. An 18% non-mechanistic reduction of A_g at the light-limited to light-saturated transition point is not likely to be an accurate representation of all of these processes. It would be better to use a more mechanistic approach, or a defensible approximation of the mechanistic approach could be developed where computational efficiency is needed.

We suggest removing CBGB smoothing from TBMs on mechanistic grounds and the evidence at hand. However, quadratic smoothing may still be preferred by some TBMs as it provides a continuous derivative to A as a function of environment, and is thus preferable for use in numerical solutions to the coupled system of equations that describe A. Where quadratic smoothing is preferred, the data suggest a value of 0.99 ± 0.011 for θ_{cj} which still would result in a reduction in A_g at the light-limited to light-saturated transition of 9.1%. We recommend at a minimum the higher value of 0.998 used by Buckley et al. (2017) that results in an A_g reduction of 4.3%.

4.2 | Influence of other processes

Electron transport, the process most commonly thought of as the key difference among FvCB and CBGB, was not a strongly influential process (10% for A and 13% for ΔA when integrated across environmental scenarios). The influence of electron transport as a process was not greater than the sum of the influence of its parameters: a, a_{jv}, b_{jv}, f and θ_j (sum of sensitivities indexes 11% for A and 16% for ΔA). That is to say, the alternative representations of electron transport did not result in appreciable between-model variability under the environmental and other conditions of the SA. This result suggests that under the conditions of this SA, a linear electron transport rate or a saturating rate with J_{max} simulated as a linear function of V_{cmax} had very little effect on simulated assimilation rates. This inference is supported by the small sensitivity indexes of a_{jv} and b_{jv} (0% and 0% integrated across models and scenarios, for A).

Our setup, based on a commonly used relationship in TBMs (Wullschleger, 1993) and a V_{cmax} value at the upper end of the range for a tropical PFT (Rogers, 2014), gave a range in the $J_{max}{:}V_{cmax}$ ratio at 25°C (JV$_{25}$) of 1.95 to 2.52. This range is fairly high, e.g. Bonan et al. (2011) used a JV ratio of 1.97, and likely contributed to the lower influence of electron transport as a process. A recent analysis

showed the JV$_{25}$ ratio to have the global range of approximately 1.0–2.5 (Kumarathunge, Medlyn, Drake, Tjoelker, et al., 2019). Nevertheless, the central values of a_{jv} and b_{jv} that we used are commonly employed by TBMs and a V_{cmax} of 50 μmol m^{-2} s^{-1} is a fairly representative value, so the parameter space of our SA is likely representative of a substantial proportion of parameter space across multiple TBMs.

Electron transport in the FvCB models also uses empirical smoothing between J_{max} and an electron transport rate that is linear with I. In models that employ non-rectangular smoothing in electron transport the parameter θ_j has a sensitivity index of 4%–8% when integrating across environmental scenarios. Smoothing of J in response to light has less influence than smoothing for limiting-rate selection because it only smooths the light response, thus can only influence the light-limited rate, while CBGB smoothing is applied to every single calculation of A. Furthermore the empirical smoothing used to represent the response to I is the best representation of that relationship currently available and lacks the mechanistic understanding and representation possible for $A_{c,g}$ using Michaelis–Menten kinetic theory (von Caemmerer, 2000).

With the addition of TPU as a limiting rate, smoothing further decreases A_g compared with using the minimum (Figure 5a). The SA suggested that the inclusion of TPU limitation as a process was not strongly influential (2% for A and 3% for ΔA when integrated across environmental scenarios). Due to the co-ordination of photosynthetic apparatus, the rate of TPU export is usually simulated as a proportion of V_{cmax} (Equation 9). Collatz et al. (1991) used a value of b_{tv} equivalent to 0.167, which is commonly used and is the central value used in this SA. Lombardozzi et al. (2018) pointed out that this value of b_{jv} may be too high based on Wullschleger (1993) and demonstrated a 9 Pg C (about 9%) smaller increase in global terrestrial ecosystem C between 1850 and 2100 in CLM4.5 under RCP8.5 when a value of 0.083 was used for b_{jv}. However, 0.083 is >1 standard error lower than the Wullschleger (1993) mean and lower than the 95% CI at 25°C from a recent synthesis (Kumarathunge, Medlyn, Drake, Rogers, & Tjoelker, 2019). Ellsworth et al. (2015) showed that TPU can be limiting under high-light and high-CO$_2$ conditions, concluding with a general recommendation that modellers interested in simulating A should consider TPU limitation (as formulated by Equation 7). However, their results demonstrate that TPU limitation is primarily influential under conditions of low O$_2$ (2%) or saturating C_i (>100 Pa). Given that these conditions are rather extreme, the low ratio of TPU to V_{cmax} chosen by Lombardozzi et al. (2018), and the results of our SA, we suggest that calculating TPU at the photosynthetic core of TBMs is probably an unnecessary computational cost.

Despite the relative lack of influence of the process of carboxylation, V_{cmax} was still the most influential parameter (i.e. accounted for more of the within-model variance than any other parameter) when models and environment were combined. This discrepancy highlights the importance of considering the variability in model process representation when conducting model SA, as illustrated by the different variances calculated by the two SA types (for A, parameter

SA variance = 0.94, while process SA variance = 2.59, despite equal means).

5 | CONCLUSIONS

At the heart of TBMs lies the surprising dominance of the non-mechanistic, limiting-rate selection process. While empirical smoothing among limiting photosynthetic rates may account for a number of mechanistic processes at various scales, it is unsatisfying that empirical functions have such influence in a model that is intended to be highly mechanistic. Indeed the FvCB model is at the core of many TBMs specifically because of its mechanistic simulation of the primary response of the terrestrial biosphere to rising CO_2 concentration, a principal driver of global change. In this SA, limiting-rate selection accounts for 65% of the variance in the CO_2 response of A. That this empirically driven variation lies within what is assumed to be a highly mechanistic process representation at the core of TBMs, it is perhaps not surprising that there is such a vast range of disagreement in Earth System model projections of the future terrestrial carbon sink. While FvCB limiting-rate selection represents selection of A at its upper bound, we suggest that this is a more defensible assumption than a highly influential non-mechanistic function with an essentially arbitrary choice of parameter values that are not supported by data.

To increase confidence in our understanding and future projections of the carbon cycle, and thus climate, we need to understand how the process representations and parameters used by TBMs drive variation in TBM simulations (Medlyn et al., 2015). Previous methods to evaluate process representations have relied on model inter-comparison projects (MIPs) either with multiple models (e.g. Anav et al., 2015; Arora et al., 2019; Walker, Hanson, et al., 2014) or comparison of alternative representations of submodels or processes within a single higher-level system model (e.g. Burrows et al., 2020). Both of these methods sample only an extremely small fraction of possible model combinations (Abramowitz & Bishop, 2014; Fisher & Koven, 2020). By allowing a fully factorial combination of models, MAAT and the process-level SA (that includes hypothesis and parameter variability) in this study represents a new frontier for model analysis and development. We investigated a small but influential component of TBMs, finding a surprising leaf-scale sensitivity that has global-scale implications. Yet the analysis presented here is just the beginning of what is possible. The quantitative multi-hypothesis tools provided by MAAT, and by other multi-hypothesis modelling groups, will help to provide rigorous advances in process-level understanding of the dynamics of complex ecosystems.

ORCID

Anthony P. Walker https://orcid.org/0000-0003-0557-5594
Abbey L. Johnson https://orcid.org/0000-0003-0338-5711
Alistair Rogers https://orcid.org/0000-0001-9262-7430
Robert A. Bridges https://orcid.org/0000-0001-7962-6329
Rosie A. Fisher https://orcid.org/0000-0003-3260-9227
Dan Lu https://orcid.org/0000-0001-5162-9843
Daniel M. Ricciuto https://orcid.org/0000-0002-3668-3021
Shawn P. Serbin https://orcid.org/0000-0003-4136-8971
Ming Ye https://orcid.org/0000-0002-7080-0578

REFERENCES

Abramowitz, G., & Bishop, C. H. (2014). Climate model dependence and the ensemble dependence transformation of CMIP projections. *Journal of Climate*, *28*(6), 2332–2348. https://doi.org/10.1175/JCLI-D-14-00364.1

Ainsworth, E. A., Davey, P. A., Hymus, G. J., Osborne, C. P., Rogers, A., Blum, H., Nosberger, J., & Long, S. P. (2003). Is stimulation of leaf photosynthesis by elevated carbon dioxide concentration maintained in the long term? A test with Lolium perenne grown for 10 years at two nitrogen fertilization levels under Free Air CO_2 Enrichment (FACE). *Plant Cell and Environment*, *26*(5), 705–714.

Anav, A., Friedlingstein, P., Beer, C., Ciais, P., Harper, A., Jones, C., Murray-Tortarolo, G., Papale, D., Parazoo, N. C., Peylin, P., Piao, S., Sitch, S., Viovy, N., Wiltshire, A., & Zhao, M. (2015). Spatiotemporal patterns of terrestrial gross primary production: A review. *Reviews of Geophysics*, *53*(3), 785–818. https://doi.org/10.1002/2015RG000483

Anderson, J., Ely, K., & Rogers, A. (2020). High density photosynthetic CO_2 response curves of hybrid poplar, New York, USA, 2019. *NGEE Tropics Data Collection*. http://doi.org/10.15486/ngt/1674983

Arora, V. K., Katavouta, A., Williams, R. G., Jones, C. D., Brovkin, V., Friedlingstein, P., Schwinger, J., Bopp, L., Boucher, O., Cadule, P., Chamberlain, M. A., Christian, J. R., Delire, C., Fisher, R. A., Hajima, T., Ilyina, T., Joetzjer, E., Kawamiya, M., Koven, C. D., … Ziehn, T. (2019). Carbon-concentration and carbon-climate feedbacks in CMIP6 models, and their comparison to CMIP5 models. *Biogeosciences Discussions*, *17*, 4173–4222. https://doi.org/10.5194/bg-2019-473

Bernacchi, C. J., Morgan, P. B., Ort, D. R., & Long, S. P. (2005). The growth of soybean under free air [CO_2] enrichment (FACE) stimulates

photosynthesis while decreasing in vivo Rubisco capacity. *Planta*, *220*(3), 434–446. https://doi.org/10.1007/s00425-004-1320-8

Beven, K. (2016). Facets of uncertainty: Epistemic uncertainty, non-stationarity, likelihood, hypothesis testing, and communication. *Hydrological Sciences Journal*, *61*(9), 1652–1665. https://doi.org/10.1080/02626667.2015.1031761

Bonan, G. B., Lawrence, P. J., Oleson, K. W., Levis, S., Jung, M., Reichstein, M., Lawrence, D. M., & Swenson, S. C. (2011). Improving canopy processes in the Community Land Model version 4 (CLM4) using global flux fields empirically inferred from FLUXNET data. *Journal of Geophysical Research: Biogeosciences*, *116*(G2), G02014. https://doi.org/10.1029/2010JG001593

Buckley, T. N., Sack, L., & Farquhar, G. D. (2017). Optimal plant water economy. *Plant, Cell & Environment*, *40*(6), 881–896. https://doi.org/10.1111/pce.12823

Burrows, S. M., Maltrud, M., Yang, X., Zhu, Q., Jeffery, N., Shi, X., Ricciuto, D., Wang, S., Bisht, G., Tang, J., Wolfe, J., Harrop, B. E., Singh, B., Brent, L., Baldwin, S., Zhou, T., Cameron-Smith, P., Keen, N., Collier, N., ... Leung L. R. (2020). The DOE E3SM v1.1 biogeochemistry configuration: Description and simulated ecosystem-climate responses to historical changes in forcing. *Journal of Advances in Modeling Earth Systems*. *12*(9), e2019MS001766. http://doi.org/10.1029/2019ms001766

Clark, D. B., Mercado, L. M., Sitch, S., Jones, C. D., Gedney, N., Best, M. J., Pryor, M., Rooney, G. G., Essery, R. L. H., Blyth, E., Boucher, O., Harding, R. J., Huntingford, C., & Cox, P. M. (2011). The Joint UK Land Environment Simulator (JULES), model description – Part 2: Carbon fluxes and vegetation dynamics. *Geoscientific Model Development*, *4*(3), 701–722. https://doi.org/10.5194/gmd-4-701-2011

Collatz, G. J., Ball, J. T., Grivet, C., & Berry, J. A. (1991). Physiological and environmental regulation of stomatal conductance, photosynthesis and transpiration – A model that includes a laminar boundary-layer. *Agricultural and Forest Meteorology*, *54*(2–4), 107–136. https://doi.org/10.1016/0168-1923(91)90002-8

Coon, E. T., David Moulton, J., & Painter, S. L. (2016). Managing complexity in simulations of land surface and near-surface processes. *Environmental Modelling & Software*, *78*, 134–149. https://doi.org/10.1016/j.envsoft.2015.12.017

Dai, H., & Ye, M. (2015). Variance-based global sensitivity analysis for multiple scenarios and models with implementation using sparse grid collocation. *Journal of Hydrology*, *528*, 286–300. https://doi.org/10.1016/j.jhydrol.2015.06.034

Dai, H., Ye, M., Walker, A. P., & Chen, X. (2017). A new process sensitivity index to identify important system processes under process model and parametric uncertainty. *Water Resources Research*, *53*(4), 3476–3490. https://doi.org/10.1002/2016WR019715

Dietze, M. C., Serbin, S. P., Davidson, C., Desai, A. R., Feng, X., Kelly, R., Kooper, R., LeBauer, D., Mantooth, J., McHenry, K., & Wang, D. (2014). A quantitative assessment of a terrestrial biosphere model's data needs across North American biomes. *Journal of Geophysical Research-Biogeosciences*, *119*(3), 286–300. https://doi.org/10.1002/2013JG002392

Ellsworth, D. S., Crous, K. Y., Lambers, H., & Cooke, J. (2015). Phosphorus recycling in photorespiration maintains high photosynthetic capacity in woody species. *Plant, Cell & Environment*, *38*(6), 1142–1156. https://doi.org/10.1111/pce.12468

Farquhar, G. D., von Caemmerer, S., & Berry, J. A. (1980). A biochemical model of photosynthetic CO_2 assimilation in leaves of C3 species. *Planta*, *149*(1), 78–90. https://doi.org/10.1007/BF00386231

Farquhar, G. D., & Wong, S. C. (1984). An empirical model of stomatal conductance. *Functional Plant Biology*, *11*(3), 191–210. https://doi.org/10.1071/pp9840191

Fisher, R. A., & Koven, C. D. (2020). Perspectives on the future of land surface models and the challenges of representing complex terrestrial systems. *Journal of Advances in Modeling Earth Systems*, *12*(4), e2018MS001453. https://doi.org/10.1029/2018MS001453

Foley, J. A., Prentice, I. C., Ramankutty, N., Levis, S., Pollard, D., Sitch, S., & Haxeltine, A. (1996). An integrated biosphere model of land surface processes, terrestrial carbon balance, and vegetation dynamics. *Global Biogeochemical Cycles*, *10*(4), 603–628. https://doi.org/10.1029/96GB02692

Gelman, A., & Rubin, D. B. (1992). Inference from iterative simulation using multiple sequences. *Statistical Science*, *7*(4), 457–472. https://doi.org/10.1214/ss/1177011136

Gu, L., Pallardy, S. G., Tu, K., Law, B. E., & Wullschleger, S. D. (2010). Reliable estimation of biochemical parameters from C3 leaf photosynthesis–intercellular carbon dioxide response curves. *Plant, Cell & Environment*, *33*(11), 1852–1874. https://doi.org/10.1111/j.1365-3040.2010.02192.x

Gupta, H. V., & Razavi, S. (2018). Revisiting the basis of sensitivity analysis for dynamical earth system models. *Water Resources Research*, *54*(11), 8692–8717. https://doi.org/10.1029/2018WR022668

Harley, P. C., & Sharkey, T. D. (1991). An improved model of C3 photosynthesis at high CO_2: Reversed O_2 sensitivity explained by lack of glycerate reentry into the chloroplast. *Photosynthesis Research*, *27*(3), 169–178. https://doi.org/10.1007/BF00035838

Harley, P. C., Thomas, R. B., Reynolds, J. F., & Strain, B. R. (1992). Modeling photosynthesis of cotton grown in elevated CO_2. *Plant Cell and Environment*, *15*(3), 271–282. https://doi.org/10.1111/j.1365-3040.1992.tb00974.x

Johnson, I. R., & Thornley, J. H. M. (1984). A model of instantaneous and daily canopy photosynthesis. *Journal of Theoretical Biology*, *107*(4), 531–545. https://doi.org/10.1016/S0022-5193(84)80131-9

Koven, C. D., Knox, R. G., Fisher, R. A., Chambers, J., Christoffersen, B. O., Davies, S. J., Detto, M., Dietze, M. C., Faybishenko, B., Holm, J., Huang, M., Kovenock, M., Kueppers, L. M., Lemieux, G., Massoud, E., McDowell, N. G., Muller-Landau, H. C., Needham, J. F., Norby, R. J., ... Chonggang, X. (2019). Benchmarking and parameter sensitivity of physiological and vegetation dynamics using the Functionally Assembled Terrestrial Ecosystem Simulator (FATES) at Barro Colorado Island, Panama. *Biogeosciences Discussions*, *17*, 3017–3044. https://doi.org/10.5194/bg-2019-409

Kull, O., & Kruijt, B. (1998). Leaf photosynthetic light response: A mechanistic model for scaling photosynthesis to leaves and canopies. *Functional Ecology*, *12*(5), 767–777. https://doi.org/10.1046/j.1365-2435.1998.00257.x

Kumarathunge, D. P., Medlyn, B. E., Drake, J. E., Rogers, A., & Tjoelker, M. G. (2019). No evidence for triose phosphate limitation of light-saturated leaf photosynthesis under current atmospheric CO_2 concentration. *Plant, Cell & Environment*, *42*(12), 3241–3252. https://doi.org/10.1111/pce.13639

Kumarathunge, D. P., Medlyn, B. E., Drake, J. E., Tjoelker, M. G., Aspinwall, M. J., Battaglia, M., Cano, F. J., Carter, K. R., Cavaleri, M. A., Cernusak, L. A., Chambers, J. Q., Crous, K. Y., De Kauwe, M. G., Dillaway, D. N., Dreyer, E., Ellsworth, D. S., Ghannoum, O., Han, Q., Hikosaka, K., ... Way, D. A. (2019). Acclimation and adaptation components of the temperature dependence of plant photosynthesis at the global scale. *New Phytologist*, *222*(2), 768–784. https://doi.org/10.1111/nph.15668

Lawrence, D. M., Fisher, R. A., Koven, C. D., Oleson, K. W., Swenson, S. C., Bonan, G., Collier, N., Ghimire, B., Kampenhout, L., Kennedy, D., Kluzek, E., Lawrence, P. J., Li, F., Li, H., Lombardozzi, D., Riley, W. J., Sacks, W. J., Shi, M., Vertenstein, M., ... Zeng, X. (2019). The Community Land Model Version 5: Description of new features, benchmarking, and impact of forcing uncertainty. *Journal of Advances in Modeling Earth Systems*, *11*(12), 4245–4287. https://doi.org/10.1029/2018MS001583

Leuning, R., Kelliher, F. M., De Pury, D. G. G., & Schulze, E.-D. (1995). Leaf nitrogen, photosynthesis, conductance and transpiration: Scaling from leaves to canopies. *Plant, Cell and Environment*, *18*(10), 1183–1200. https://doi.org/10.1111/j.1365-3040.1995.tb00628.x

Lin, Y.-S., Medlyn, B. E., Duursma, R. A., Prentice, I. C., Wang, H., Baig, S., Eamus, D., de Dios, V. R., Mitchell, P., Ellsworth, D. S., de Beeck, M. O., Wallin, G., Uddling, J., Tarvainen, L., Linderson, M.-L., Cernusak, L. A., Nippert, J. B., Ocheltree, T. W., Tissue, D. T., … Wingate, L. (2015). Optimal stomatal behaviour around the world. *Nature Climate Change*, *5*(5), 459–464. https://doi.org/10.1038/nclimate2550

Lombardozzi, D. L., Smith, N. G., Cheng, S. J., Dukes, J. S., Sharkey, T. D., Rogers, A., Fisher, R., & Bonan, G. B. (2018). Triose phosphate limitation in photosynthesis models reduces leaf photosynthesis and global terrestrial carbon storage. *Environmental Research Letters*, *13*(7), 074025. https://doi.org/10.1088/1748-9326/aacf68

Maire, V., Martre, P., Kattge, J., Gastal, F., Esser, G., Fontaine, S., & Soussana, J.-F. (2012). The coordination of leaf photosynthesis links C and N fluxes in C3 plant species. *PLoS ONE*, *7*(6), e38345. https://doi.org/10.1371/journal.pone.0038345

Medlyn, B. E., Duursma, R. A., Eamus, D., Ellsworth, D. S., Prentice, I. C., Barton, C. V. M., Crous, K. Y., De angelis, P., Freeman, M., & Wingate, L. (2011). Reconciling the optimal and empirical approaches to modelling stomatal conductance. *Global Change Biology*, *17*(6), 2134–2144. https://doi.org/10.1111/j.1365-2486.2010.02375.x

Medlyn, B. E., Zaehle, S., De Kauwe, M. G., Walker, A. P., Dietze, M. C., Hanson, P. J., Hickler, T., Jain, A. K., Luo, Y., Parton, W., Prentice, I. C., Thornton, P. E., Wang, S., Wang, Y.-P., Weng, E., Iversen, C. M., McCarthy, H. R., Warren, J. M., Oren, R., & Norby, R. J. (2015). Using ecosystem experiments to improve vegetation models. *Nature Climate Change*, *5*(6), 528–534. https://doi.org/10.1038/nclimate2621

Oleson, K. W., Lawrence, D. M., Bonan, G. B., Levis, S., Swenson, S. C., Thornton, P. E., Bozbiyik, A., Fisher, R. A., Heald, C. L., Kluzek, E., Lamarque, J.-F., Lawrence, P. J., Lipscomb, W., Muszala, S. P., Sachs, W. J., Drewniak, B., Huang, M., Koven, C. D., Li, F., … Yang, Z. (2013). *Technical Description of version 4.5 of the Community Land Model (CLM) (TN-503+STR; NCAR Technical Note)*. National Centre for Atmospheric Research.

R Core Team. (2020). *R: A language and environment for statistical computing*. R Foundation for Statistical Computing. Retrieved from https://www.R-project.org/

Ricciuto, D., Sargsyan, K., & Thornton, P. (2018). The impact of parametric uncertainties on biogeochemistry in the E3SM land model. *Journal of Advances in Modeling Earth Systems*, *10*(2), 297–319. https://doi.org/10.1002/2017MS000962

Rogers, A. (2014). The use and misuse of $V_{c,max}$ in earth system models. *Photosynthesis Research*, *119*(1–2), 15–29. https://doi.org/10.1007/s11120-013-9818-1

Rogers, A., Medlyn, B. E., Dukes, J. S., Bonan, G., von Caemmerer, S., Dietze, M. C., Kattge, J., Leakey, A. D. B., Mercado, L. M., Niinemets, Ü., Prentice, I. C., Serbin, S. P., Sitch, S., Way, D. A., & Zaehle, S. (2017). A roadmap for improving the representation of photosynthesis in Earth system models. *New Phytologist*, *213*(1), 22–42. https://doi.org/10.1111/nph.14283

Rogers, A., Serbin, S. P., Ely, K. S., Sloan, V. L., & Wullschleger, S. D. (2017). Terrestrial biosphere models underestimate photosynthetic capacity and CO_2 assimilation in the Arctic. *New Phytologist*, *216*(4), 1090–1103. https://doi.org/10.1111/nph.14740

Saltelli, A., Annoni, P., Azzini, I., Campolongo, F., Ratto, M., & Tarantola, S. (2010). Variance based sensitivity analysis of model output. Design and estimator for the total sensitivity index. *Computer Physics Communications*, *181*(2), 259–270.

Sharkey, T. D. (1985). Photosynthesis in intact leaves of C3 plants: Physics, physiology and rate limitations. *The Botanical Review*, *51*(1), 53–105. https://doi.org/10.1007/BF02861058

Smith, E. L. (1937). The influence of light and carbon dioxide on photosynthesis. *The Journal of General Physiology*, *20*(6), 807–830. https://doi.org/10.1085/jgp.20.6.807

Smith, N. G., Keenan, T. F., Colin Prentice, I., Wang, H., Wright, I. J., Niinemets, Ü., Crous, K. Y., Domingues, T. F., Guerrieri, R., Yoko Ishida, F., Kattge, J., Kruger, E. L., Maire, V., Rogers, A., Serbin, S. P., Tarvainen, L., Togashi, H. F., Townsend, P. A., Wang, M., … Zhou, S.-X. (2019). Global photosynthetic capacity is optimized to the environment. *Ecology Letters*, *22*(3), 506–517. https://doi.org/10.1111/ele.13210

von Caemmerer, S. (2000). *Biochemical models of leaf photosynthesis*. CSIRO Publishing.

Vrugt, J. A. (2016). Markov chain Monte Carlo simulation using the DREAM software package: Theory, concepts, and MATLAB implementation. *Environmental Modelling & Software*, *75*, 273–316. https://doi.org/10.1016/j.envsoft.2015.08.013

Vrugt, J. A., ter Braak, C. J. F., Diks, C. G. H., Robinson, B. A., Hyman, J. M., & Higdon, D. (2009). Accelerating Markov chain Monte Carlo simulation by differential evolution with self-adaptive randomized subspace sampling. *International Journal of Nonlinear Sciences and Numerical Simulation*, *10*(3), 273–290. https://doi.org/10.1515/IJNSNS.2009.10.3.273

Walker, A. P., Beckerman, A. P., Gu, L., Kattge, J., Cernusak, L. A., Domingues, T. F., Scales, J. C., Wohlfahrt, G., Wullschleger, S. D., & Ian Woodward, F. (2014). The relationship of leaf photosynthetic traits – V_{cmax} and J_{max} – to leaf nitrogen, leaf phosphorus, and specific leaf area: A meta-analysis and modeling study. *Ecology and Evolution*, *4*(16), 3218–3235. https://doi.org/10.1002/ece3.1173

Walker, A., Fisher, R., & Ricciuto, D. (2020). Global gross primary production simulated by three terrestrial biosphere models to analyse smoothing of limiting rates. *Next-Generation Ecosystem Experiments (NGEE) Tropics*. https://data.ess-dive.lbl.gov/view/doi:10.15485/1682253

Walker, A. P., Hanson, P. J., De Kauwe, M. G., Medlyn, B. E., Zaehle, S., Asao, S., Dietze, M., Hickler, T., Huntingford, C., Iversen, C. M., Jain, A., Lomas, M., Luo, Y., McCarthy, H., Parton, W. J., Colin Prentice, I., Thornton, P. E., Wang, S., Wang, Y.-P., … Norby, R. J. (2014). Comprehensive ecosystem model-data synthesis using multiple data sets at two temperate forest free-air CO_2 enrichment experiments: Model performance at ambient CO_2 concentration. *Journal of Geophysical Research: Biogeosciences*, *119*(5), 937–964. https://doi.org/10.1002/2013JG002553

Walker, A. P., Lu, D., & Ye, M. (2020). Leaf-scale carbon assimilation simulated by the multi-assumption architecture & testbed for process sensitivity analysis. *Climate Change-Terrestrial Ecosystem Science SFA*. https://data.ess-dive.lbl.gov/view/doi:10.15485/1682250

Walker, A. P., Quaife, T., van Bodegom, P. M., De Kauwe, M. G., Keenan, T. F., Joiner, J., Lomas, M. R., MacBean, N., Xu, C., Yang, X., & Ian Woodward, F. (2017). The impact of alternative trait-scaling hypotheses for the maximum photosynthetic carboxylation rate (Vcmax) on global gross primary production. *New Phytologist*, *215*(4), 1370–1386. https://doi.org/10.1111/nph.14623

Walker, A. P., Ye, M., Lu, D., De Kauwe, M. G., Gu, L., Medlyn, B. E., Rogers, A., & Serbin, S. P. (2018). The multi-assumption architecture and testbed (MAAT v1.0): R code for generating ensembles with dynamic model structure and analysis of epistemic uncertainty from multiple sources. *Geoscientific Model Development*, *11*(8), 3159–3185. https://doi.org/10.5194/gmd-11-3159-2018

Wang, H., Prentice, I. C., Keenan, T. F., Davis, T. W., Wright, I. J., Cornwell, W. K., Evans, B. J., & Peng, C. (2017). Towards a universal model

for carbon dioxide uptake by plants. *Nature Plants*, *3*(9), 734–741. https://doi.org/10.1038/s41477-017-0006-8

Woodward, F. I., & Lomas, M. R. (2004). Vegetation dynamics – Simulating responses to climatic change. *Biological Reviews*, *79*(3), 643–670. https://doi.org/10.1017/S1464793103006419

Wullschleger, S. D. (1993). Biochemical limitations to carbon assimilation in C3 plants—A retrospective analysis of the A/Ci curves from 109 species. *Journal of Experimental Botany*, *44*(5), 907–920. https://doi.org/10.1093/jxb/44.5.907

Zaehle, S., Sitch, S., Smith, B., & Hatterman, F. (2005). Effects of parameter uncertainties on the modeling of terrestrial biosphere dynamics. *Global Biogeochemical Cycles*, *19*(3), GB3020. https://doi.org/10.1029/2004GB002395

SUPPORTING INFORMATION

Additional supporting information may be found online in the Supporting Information section.